



Article

Quasi-Static Sliding Wear Analysis of 3D Rough Surface Considering Changes in the Point of Contact

Yunji Kim ^{1,†} , Junho Suh ^{2,†} , Bora Lee ², Yondo Chun ³ , Keejun Park ⁴ and Yonghun Yu ^{4,*}¹ LG Energy Solution, Daejeon 34122, Republic of Korea² School of Mechanical Engineering, Pusan National University, Busan 46241, Republic of Korea³ Electric Machines and Drives System Research Center, Korea Electrotechnology Research Institute, Changwon 51543, Republic of Korea⁴ Innovative Transportation & Logistics Research Center, Korea Railroad Research Institute, Uiwang-si 16105, Republic of Korea

* Correspondence: yonghunyu87@krii.re.kr

† These authors contributed equally to this work.

Abstract: This study analyzed adhesive wear in periodic sliding motion using a quasi-static deterministic wear model that considered changes in the point of contact of asperities as well as changes in the surface and statistical parameters. The contact pressure was calculated using the semi-analytical method (SAM) based on the periodic properties of the rough surface, and the wear was analyzed by obtaining the wear depth for each node using the Archard wear model. We took into account that the sliding distances of the upper moving surface and the lower stationary surface are different according to the actual size of the two objects. We compared the results of the quasi-static wear analysis with the truncation model and the deterministic fixed model, which did not consider the change in the asperity contact point. In the truncation model, an error in the estimation of the radius occurred in the process of fitting the tip of asperities with a sphere. As the asperities became flatter by wear, this error accumulated, which revealed a difference in the deterministic wear analysis results. As a result of the wear analysis on the periodic surface, the RMS roughness of the positively skewed surface decreased the fastest, the skewness increased in the negative direction, and the kurtosis initially decreased and then increased. In addition, wear scars occurred due to the difference in wear depth between the lower stationary surface and the upper moving surface.

Keywords: point of contact; quasi-static deterministic wear model; SAM; sliding wear

Citation: Kim, Y.; Suh, J.; Lee, B.; Chun, Y.; Park, K.; Yu, Y. Quasi-Static Sliding Wear Analysis of 3D Rough Surface Considering Changes in the Point of Contact. *Appl. Sci.* **2022**, *12*, 12465. <https://doi.org/10.3390/app122312465>

Academic Editors: Carlos M.C.G. Fernandes and Pedro M.T. Marques

Received: 9 November 2022

Accepted: 29 November 2022

Published: 6 December 2022

Publisher's Note: MDPI stays neutral with regard to jurisdictional claims in published maps and institutional affiliations.



Copyright: © 2022 by the authors. Licensee MDPI, Basel, Switzerland. This article is an open access article distributed under the terms and conditions of the Creative Commons Attribution (CC BY) license (<https://creativecommons.org/licenses/by/4.0/>).

1. Introduction

Sliding wear is a major problem commonly encountered in a variety of engineering problems. Over the past few decades, the most difficulty in mechanical design has been encountered in achieving the required performance that corresponds to the beginning of the Bathtub curve of the product. However, with rapid advances in science, technology, and computing power, the cost of solving these initial deficiencies has significantly decreased. On the other hand, as the recognition of the importance of product reliability is increasing gradually, failure due to repeated use of mechanical components is one of the research topics that is currently receiving the most attention. Typical examples of failure caused by repeated use are wear and fatigue failure, and fatigue failure is also greatly affected by wear [1]. Holmberg closely analyzed the economic losses from wear, and the amount was found to be enormous [2]. Not only from an economic point of view but also from a biomedical engineering and environmental point of view, wear is a factor that must be reduced. For example, it is recognized that the biggest problem with joint replacement surgery is wear. If wear debris enters a sliding surface, the lifespan of the artificial joint is greatly shortened, and in severe cases, failure may occur [3]. In terms of environmental pollution, approximately 35% of wear particles generated from brake pads are emitted as

fine dust PM10 in the air [4] and cause environmental pollution along with the fine dust generated by tire and road wear [5–7].

As the problems caused by wear become more important, related studies are being actively conducted. To reduce wear, efforts are being made to experimentally verify the effect of wear reduction through the application of new materials [8–10], coating [11–15], heat treatment [16,17], and texturing [18,19] in a wide variety of environments.

Nevertheless, it is very difficult to obtain accurate data from the wear test for the following reasons: (1) It takes a great deal of time and (2) the result has a large dispersion. In addition to the difficulty of data acquisition itself, there is also a problem in identifying the main parameters that cause wear because changes in the surface and interaction at the interface during the process are unknown. On the other hand, numerical analysis of wear based on the generated surface is economical because it takes less time and does not require additional processing such as noise removal or equipment required for the experiment. It also has the advantage of being able to observe changes in the surface as wear progresses.

Numerical wear analysis consists of procedures for calculating the contact pressure and then calculating the wear depth. The method of calculating the contact pressure is divided into a deterministic method and a probabilistic method. The former method calculates the wear depth at each node after calculating the pressure using the semi-analytical method (SAM) [20,21], and the latter method statistically calculates the average contact pressure based on the Greenwood–Williamson (GW) model and then analyzes the wear depth using the truncation model [22,23]. The concept of the truncation model is to obtain the average wear depth over the entire surface and cut the surface profile into a rigid plane. Thomas, who first proposed the truncation model, analyzed the wear of a Gaussian surface by setting 10% of the height difference between the highest and the lowest points of the surface profile as the wear depth [24]. Spedding applied the Pearson system to analyze wear on a non-Gaussian surface [25], and Stout used Spedding's model to observe the change in the root mean square (RMS) roughness of the engine bore [26]. Considering the extreme skewness and kurtosis values of numerous worn surfaces, they showed that the wear of cylinder liners and bores can be predicted through the truncation model. Ghosh used an average wear model similar to the truncation model for wear analysis of 2D surface profiles [23]. This model determines the contact node by setting the rigid body displacement, and then calculates the average wear depth with the Archard wear model based on the contact pressure. Since the contact pressure is obtained using the Hertzian contact solution, the asperity radius must be approximated for each contact asperity. Greenwood and Williamson, who proposed a stochastic rough surface contact model, determined the radius using the '3-point peak' method of fitting the peak and adjacent points with a parabola [27], and Majumdar and Bhushan simplified the calculation by assuming that the asperities shape is a sphere [28]. Ghosh used the intersections of the rigid plane-surface profile detected by the algorithm for the radius assumption, and when multiple asperities were in contact, the peak height distribution was reflected in the approximated asperity radius [23]. They analyzed wear on rough surfaces with a wide range of RMS roughness, skewness, and kurtosis. As a result, high wear rates were observed on positively skewed, high-kurtosis surfaces, and wear regimes of severe and mild wear were observed. Prajapati developed a numerical 3D wear model by extending Ghosh's model to elastic–plastic contact and observed changes in parameters that occur during the wear process. The results of the wear analysis of the surface with the same characteristics as the specimen were in good agreement with the experimental results [22].

If the deterministic method is used, more precise wear analysis is possible compared to the statistical method. The main reason is that since deterministic wear analysis deals with the actual rough surface itself, the assumptions used in statistical methods such as fitting asperities into a spherical shape in the process of contact pressure calculation or calculating the average wear depth are no longer necessary. Since the contact pressure only varies greatly depending on the surface shape but is also the main factor that governs the wear depth, the surface shape must be reflected as it is in the process of contact pressure

calculation. In that way, the change in the contact area, the shape of the worn asperities, and the surface parameters of the worn surface can be obtained in detail. Zhu analyzed wear under elastohydrodynamic lubrication (EHL) through a deterministic method and suggested a method of calibrating the wear coefficient by comparing it with the experiment, and also found that the surface change and wear scar shown in the analysis results were in good agreement with the experiment [29]. Pei predicted the surface topography and friction coefficient in rolling-sliding contact under mixed lubrication conditions using Zhu's model and showed that the slide-to-roll ratio had a great influence on the wear rate [21]. Zhang analyzed torsional fretting wear using SAM [20].

In a real phenomenon, the asperity passes over the asperity on the opposite surface and the point of contact changes with time. In most of the existing studies on rough surface wear, the relative point of contact of the asperities does not change, so the wear depth at some locations may be overestimated. Therefore, it is necessary to consider the movement of asperities so as to obtain a result more similar to reality. Pei analyzed the sliding wear by moving the disk a small distance at each time step to analyze the wear of the ball-on-disk in rolling-sliding contact under mixed lubrication and intensively analyzed the surface topography evolution and friction coefficient [21]. Brink also considered the motion of asperities in the same way [30], and they used the wear mechanism proposed by Aghababaei, which states that wear particles are generated when the energy between sliding surfaces is sufficient to overcome the kinetic barriers [31]. Aghababaei's model is also consistent with Rabinowicz's hypothesis that wear particles are generated in the asperities where a strong junction occurs when two surfaces slide against each other [32]. Brink's model has the great advantage that it does not require a wear coefficient to be measured experimentally, but it has not been sufficiently verified due to the lack of detailed experimental data.

In this study, we performed a deterministic quasi-static wear analysis considering the point of contact that changed according to the sliding of asperities on two rough surfaces in relative motion, and also analyzed the evolution of surface topography and parameters representing the surface. We used the continuous convolution Fourier transform (CC-FT) for contact analysis of periodic rough surfaces and the Archard wear model to calculate the wear depth. In addition, we compared the differences in the analysis results between the truncation model, the deterministic fixed wear model that does not consider the change in the point of contact (referred to as the fixed model), and the deterministic quasi-static wear model that considers the change in the point of contact (referred to as the quasi-static model).

2. Theoretical Background

2.1. Problem Description and Hypotheses

Figure 1 shows the periodic sliding motion between two objects with apparently flat contact surfaces. In this case, it is assumed that the sliding speed is constant and the load acts in the direction perpendicular to the contact surface. In a sliding motion such as that in Figure 1, the contact surface of the upper moving body with length L_M in the sliding direction is not changed, whereas the contact surface of the lower stationary body with length L_S in the sliding direction varies over time. The contact surfaces are called the upper moving surface and the lower stationary surface.

Since a very dense grid is required to represent the rough surface asperities, the analysis domain must be carefully set. Depending on the object, the area of the contact surface varies from micro-scale to metric-scale. The larger the contact surface area, the longer the analysis time and the higher the computer cost. On the other hand, reducing the number of nodes increases the sampling interval, making it impossible to accurately represent rough surfaces. That is, the analysis domain should be selected as an area that minimizes the computational burden while having a grid size that sufficiently represents the roughness of the surface including numerous asperities.

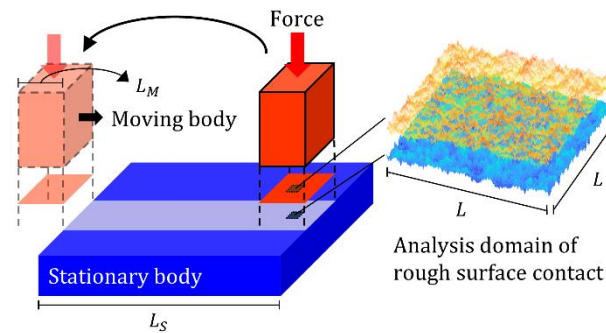


Figure 1. Schematic of periodic sliding motion between a lower stationary body and an upper moving body under constant normal force.

Therefore, the analysis domain is limited to a very small area at the level where the periodicity of the rough surface is held among the total contact area. In order to select such an appropriate analysis domain, it is necessary to establish a standard. Parameters representing rough surfaces include statistical parameters for height distribution and autocorrelation function that provides information about spatial distribution. The autocorrelation function (ACF) represents the spatial correlation of the rough surface height and is expressed as the following equation [33].

$$R(\Delta x, \Delta y) = \mathbb{E}\{z(x, y)z(x + \Delta x, y + \Delta y)\} \quad (1)$$

where \mathbb{E} is the expectation operator and z is the rough surface height. Equation (1) means that the autocorrelation function indicates the degree of correlation between the height at an arbitrary point and the height at a point at a distance of Δx in the x direction and Δy in the y direction. It is known that most autocorrelation functions of engineering surfaces have the form of exponential functions [34]. An important parameter for the autocorrelation function is the autocorrelation length β , which is mainly defined as the length to the point at which the value of the autocorrelation function is 0.1 [33]. For a numerical generation of rough surfaces, it is assumed that the autocorrelation function has a value of zero after a certain length, where this length is the truncation length [35]. In a past study on rough surface generation, the truncation length was arbitrarily determined, but in He's work, it was reported that the truncation length should be 6 or more times the value of β to obtain an accurate surface without losing statistical information [35]. Therefore, since the minimum surface length for given statistical and spatial information is equal to the truncation length, in this study, we set the truncation length to be more than 10 times β and the length of the analysis domain L to be twice the truncation length to ensure a sufficient surface grid.

The most significant feature of the analysis method we used in this study was that, in the model, we took into account that the point of contact changes according to the relative motion of the asperities. This phenomenon was implemented by the direct movement of the data. As shown in Figure 2, in this process, the data of the upper moving surface are stacked on top of the data of the lower stationary surface, and the data of the upper moving surface are shifted by δ_s in the sliding direction to consider the movement of asperities. According to the periodicity of the rough surface, the lower stationary surface data outside the analysis domain are inserted on the opposite side. A detailed description of the periodicity is described later.

By dividing one sliding cycle into small steps and analyzing each step, the sliding process becomes a quasi-static process, and the upper moving surface moves to the right by δ_s at each step. δ_s is an integer multiple of the sampling interval Δ . As δ_s increases, the number of contact analyses decreases, which is beneficial in terms of analysis time. However, the smaller the value of δ_s , the more detailed the effect of the movement of the projection can be. In this study, we selected Δ , the smallest movement unit, as δ_s .

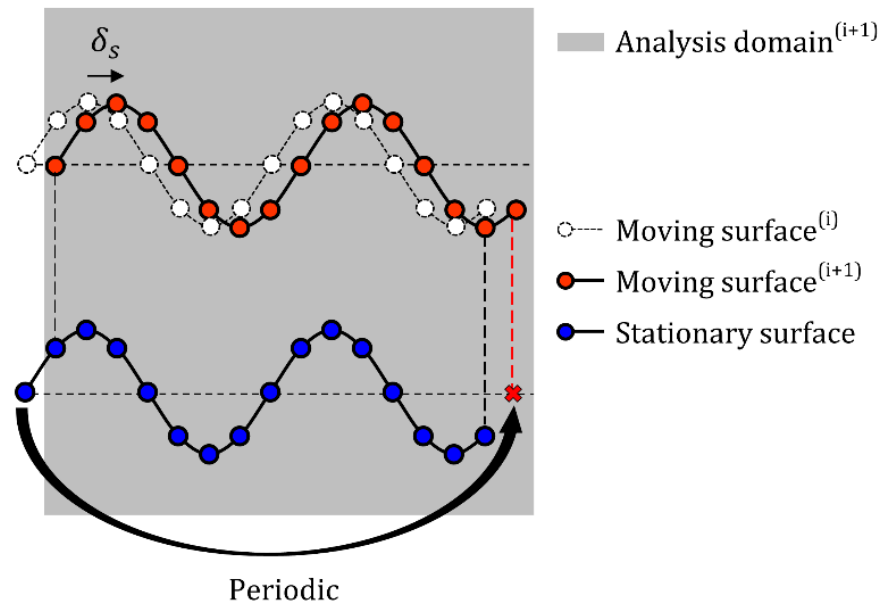


Figure 2. Schematic of data movement to account for changing contact points of asperities.

2.2. Contact Model

Deterministic solutions to rough surface contact problems include the direct method, multi-level multi-summation, and the conjugate gradient method (CGM). In the process of the CGM, the contact problem can be solved quickly and efficiently if CC-FT is coupled based on the periodic nature of the rough surface. In the discrete convolution fast Fourier transform (DC-FFT), which deals with non-periodic problems, the domain length needs to be doubled. Periodic problems can also be solved with the DC-FFT, but it is inefficient because the domain must be extended [36].

In the elastic contact problem, the following inequalities and constraints must be satisfied and can be solved by the CGM. For further details, refer to [37].

$$\sum_{(k,l) \in I_g} K_{i-k,j-l} p_{k,l} = h_{i,j} + \alpha \quad (i, j) \in I_c \tag{2}$$

$$p_{i,j} > 0 \quad (i, j) \in I_c \tag{3}$$

$$\sum_{(k,l) \in I_g} K_{i-k,j-l} p_{k,l} \geq h_{i,j} + \alpha \quad (i, j) \notin I_c \tag{4}$$

$$p_{i,j} = 0 \quad (i, j) \notin I_c \tag{5}$$

$$\sum_{(i,j) \in I_g} p_{i,j} dx dy = F_z \tag{6}$$

where K is the influence coefficient, p is the pressure, h is the gap between the two surfaces, α is the rigid body displacement, I_g is the set of all nodes in the analysis domain, I_c is the set of nodes in contact, and F_z is the normal load. The convolution terms in Equations (2) and (4) are the elastic deformation u due to pressure, which can be efficiently obtained by the CC-FT.

$$u = IDFT\left(\tilde{G} \cdot \tilde{p}\right) \tag{7}$$

where \tilde{G} is the frequency response function (FRF) and \tilde{p} is the Fourier transformed pressure. According to the nature of the CC-FT, all values related to the CC-FT are repeated with the same period as the profile of the rough surface. That is, the surface height, elastic deformation, and pressure are also periodic functions with a period of L , which is the total length of the analysis domain.

It is known that the asperity of the rough surface is initially plastically deformed [38]. In order to capture a plastic behavior, it is necessary to perform an elastic–plastic contact analysis. The elastic–plastic contact analysis is divided into elastic–perfectly plastic (EPP) and elastic–plastic (EP) according to the stress–strain curve [36]. EP is a model that considers the change in contact pressure due to plastic deformation under the surface. On the other hand, EPP is a simple method of setting the pressure to be equal to the hardness if the contact pressure exceeds the hardness of the softer material [39]. In order to reduce the computational burden, the EPP method, which does not require the stress analysis of the subsurface, is adopted in the current model.

2.3. Wear Model

This section describes the wear analysis method using the truncation model and the wear analysis method using the deterministic model considering the change in the asperities contact points. First, as inferred from the name, the truncation model is a method of analyzing wear by cutting the asperities in contact with a rigid plane, and the analysis proceeds with the following procedure: (1) The contact between two rough surfaces is replaced by the contact between the rough surface and the rigid plane. (2) After detecting the contact asperities by the displacement of the rigid body and the surface profile, the contact pressure of the asperity is calculated using the Greenwood–Willamson statistical method based on the Hertzian contact theory. The method of calculating the contact pressure of the asperity is described in detail in Section 3.1. (3) The wear depth is obtained using the Archard wear model. (4) The average wear depth for the entire surface is calculated, and the height of the nodes in contact is replaced with the value of maximum surface height minus average wear depth. The truncation model is one of the methods currently widely used in wear analysis due to its convenience. However, there is a disadvantage in that the initially formed contact points of the asperities do not change and the wear at the arbitrary location is overestimated.

The quasi-static model supplements the shortcomings of the truncation model, considering the change in the point of contact and the pressure distribution of the asperity as the surface slides. This makes it possible to perform the wear analysis on each of the moving and stationary surfaces separately, which means that the wear analysis is possible when the physical properties and wear resistance of the two surfaces are different. The wear depth at each node in contact is calculated with the modified Archard wear model, and the equation is:

$$h_{w_i}(x, y) = \frac{k_i p(x, y) s_i}{H_i} \quad (i = 1, 2) \quad (8)$$

where h_w is the wear depth, k is the wear coefficient, p is the contact pressure, s is the sliding distance, H is the hardness, $i = 1$ is the upper moving surface, and $i = 2$ is the lower stationary surface. According to the Archard wear equation, since wear depth is highly dependent on contact pressure, the statistical contact analysis is replaced with a deterministic method to calculate the contact pressure between rough surfaces more accurately. The surface profile is updated by subtracting (removing) the wear depth of each node obtained through Equation (8) from the previous surface height. By averaging the pressure distributions calculated in each step, the average pressure for 1 cycle at each node is obtained and then used for the wear analysis. It should be noted that since the lower stationary surface is not in constant contact, the sliding distance is smaller than that of the upper moving surface, resulting in a relatively small amount of wear depth on the lower stationary surface. When the upper moving surface slides by the sliding distance S , the lower stationary surface slides by the length of the upper moving body L_M . Based on this, the wear depth is calculated by varying the sliding distance between the two surfaces. This wear analysis model was also used in this literature [21] to study the influence of the surface topography, load, and slide-to-roll ratio on wear, and the analysis results were verified with experiments.

2.4. Numerical Procedure

Figure 3 shows the flowchart of wear analysis, and the process is summarized as follows.

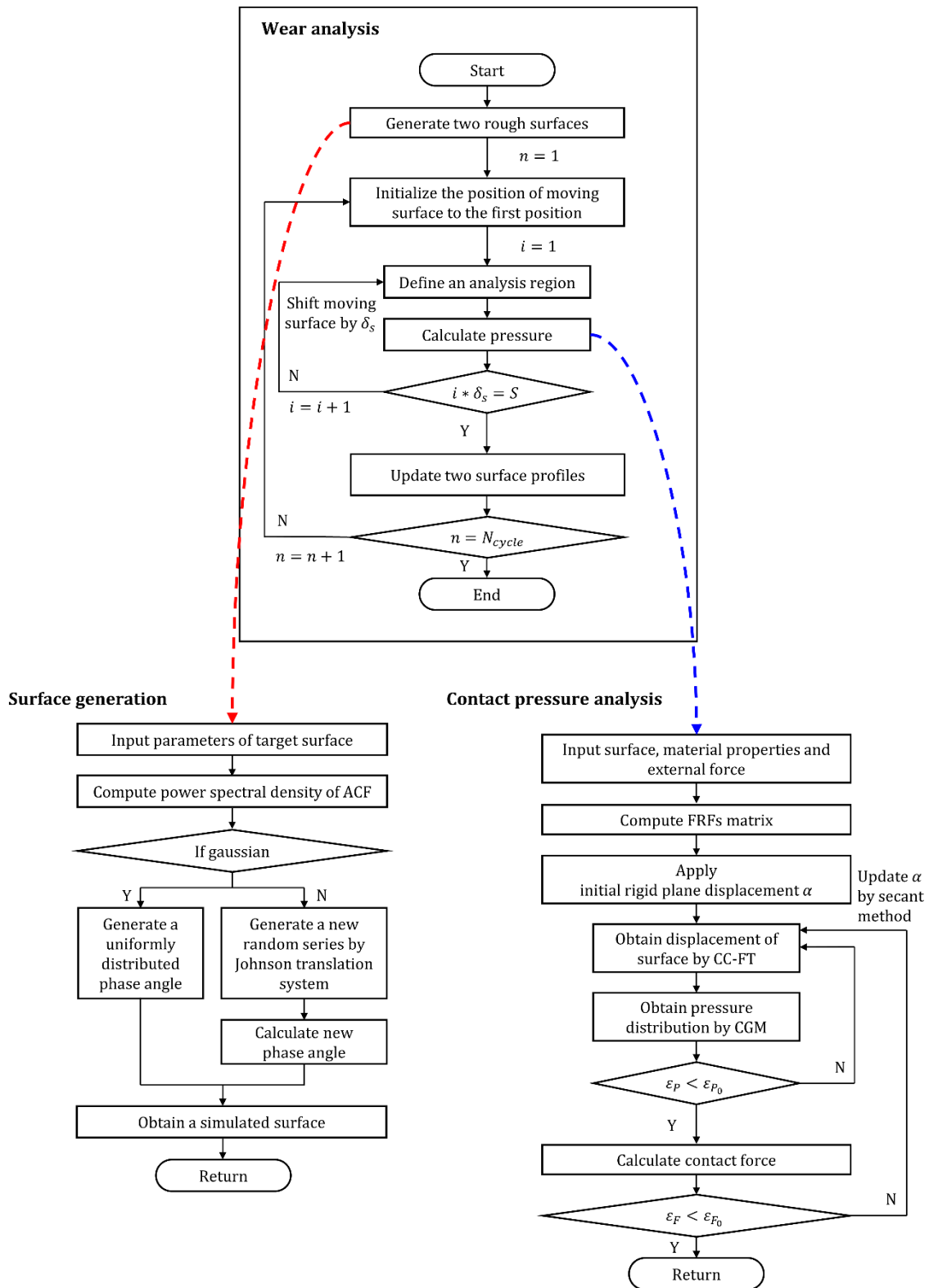


Figure 3. Flowchart of numerical analysis for rough surface wear using deterministic quasi-static wear model.

- (1) Generate a rough surface numerically based on the roughness parameters and ACF. For detailed methods of numerical generation of rough surfaces with Gaussian and non-Gaussian distributions, see [40,41].
- (2-1) Align the upper moving surface with the lower stationary surface and set the analysis domain.
- (2-2) Calculate the contact pressure of the analysis domain using CGM and CC-FT.
- (2-3) Move the upper moving surface by δ_s , and insert the data of the lower stationary surface outside the analysis area into the opposite side.
- (2-4) Repeat the contact analysis while moving the upper moving surface until the total amount of movement is the sliding distance S .
- (3) After step (2), the surface profile is updated for each surface node using the calculated wear depth based on the average pressure during sliding.

After steps (2) and (3) are repeated up to the set number of cycles N_{cycle} , the worn profile is obtained.

3. Result and Discussion

3.1. Comparison between Three Wear Models

Before performing the wear analysis on the rough surface using the truncation model and the deterministic model introduced in Section 2.3, we compared the results on the sliding wear of a plane and one spherical asperity for a basic analysis between the models. The analysis results of the following three models were compared: The truncation model, the deterministic fixed model, and the deterministic quasi-static model. The deterministic model includes a fixed model that does not consider the change in the asperity contact point, such as the assumption of the truncation model, and a quasi-static model that considers the change in the asperity contact point. The truncation model and the deterministic fixed model differ only in the pressure calculation method.

The deterministic model obtains the pressure at each node based on a deterministic method. DC-FFT was used as a numerical analysis technique for the non-periodic contact problem because CC-FT, which was used for the rough surface contact analysis, cannot be used in the case of a sphere contact. More details on this can be found in [42].

The truncation model is the simplest model that calculates the contact pressure based on the GW model and does not consider the change in the asperity contact point. In the truncation model, assuming that the tip of each asperity is spherical, the contact load F and contact area A were calculated according to the Hertzian contact theory with the following equation [43].

$$F = \begin{cases} \frac{4}{3}E'R'^{0.5}\omega^{1.5} & \omega < \omega_c \\ \pi R'\omega(2 - \frac{\omega_c}{\omega})k_{ep}H & \omega > \omega_c \end{cases} \quad (9)$$

$$A = \begin{cases} \pi R'\omega & \omega < \omega_c \\ \pi R'\omega(2 - \frac{\omega_c}{\omega}) & \omega > \omega_c \end{cases}$$

Here, $E' = 1/((1 - \nu_1^2)/E_1 + (1 - \nu_2^2)/E_2)$ is the equivalent Young's modulus, R' is the equivalent radius of asperity, ω is the amount of interference between the rigid plane-surface, k_{ep} is the elastic-plastic constant, and if ω is greater than $\omega_c = \left(\frac{\pi k_{ep}H}{2E'}\right)^2 R'$, the asperity is considered to be plastically deformed [43]. The radius of the asperity is determined by its geometry, and as the radius increases as the wear progresses, the radius must be newly estimated every cycle. After the radius of asperity based on the 2D profile in the x direction and y direction is calculated, the equivalent radius $R' = \sqrt{R'_x R'_y}$ is obtained from the two radii. To calculate R'_x, R'_y , a circle is fitted using the two intersection points of the rigid plane-surface profile and the highest point of the asperity. In the truncation model, since the asperities are cut horizontally, a flat area is quickly formed at the tip of the asperities. For the worn asperities, the midpoint of the flat area is set as the peak point.

Figure 4 shows the wear process for 1000 cycles for a sphere with an equivalent elastic modulus of $E' = 110$ GPa, Poisson's ratio of $\nu = 0.3$, and an equivalent radius of

$R' = 300$ mm slides on a rigid plane under a normal load of 410 kN. The wear coefficient is $k = 5 \times 10^{-5}$, and the sliding distance per cycle is $S = 1$ mm. As a result of contact analysis on the unworn surface, the maximum pressure was calculated as 2.2 GPa in all three models, which was consistent with the Hertz contact theory.

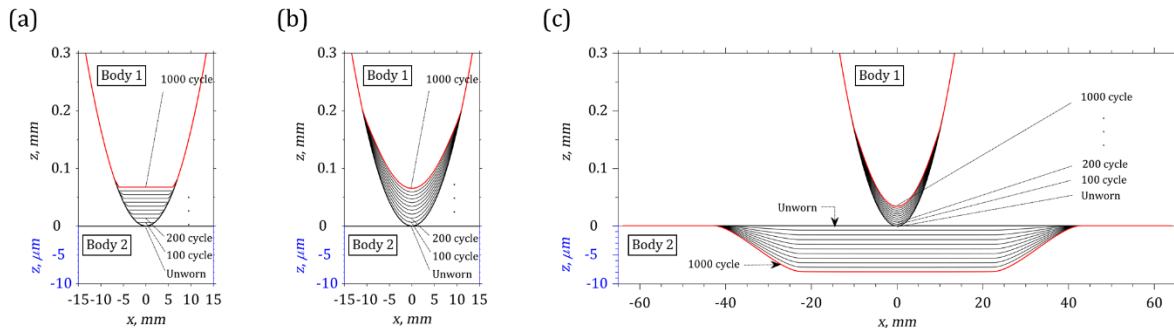


Figure 4. Wear profile for sliding wear of a single asperity with an equivalent elastic modulus of $E' = 110$ GPa, Poisson's ratio $\nu = 0.3$, and an equivalent radius of $R' = 300$ mm under a normal load of 410 kN: (a) Truncation model; (b) deterministic fixed model; (c) deterministic quasi-static model.

In the truncation model and the fixed model, which do not consider the change in contact point, wear continues to occur at the same point. Since the gap between the two surfaces (equivalent surface) does not change during one cycle, the wear depth of the two models was compared based on the equivalent surface.

After 1000 cycles, the wear depth at the peak of the sphere was $68.3 \mu\text{m}$ in the truncation model and $65.9 \mu\text{m}$ in the fixed model, and the truncation model's prediction is 3.6% greater. In the fixed model, the surface profile itself is used for calculating the pressure, but in the truncated model, it is a cause of error to assume that the tip of the worn asperity is a sphere. Since the point of the flat area is used for fitting in the step of assuming the worn asperity as a sphere, the profile of the fitted asperity becomes a circle inscribed with the real profile of the worn asperity. Therefore, comparing the volume of the fitted sphere with the volume of the actual asperity with worn tips, the former is smaller. This results in the radius being estimated to be small in the analysis, and the contact area is smaller than the real one. Therefore, in the truncation model, the maximum pressure is greater than in the fixed model, which results in greater wear depth. On the other hand, in the quasi-static model, since the gap between the two surfaces (corresponding surface) changes as the upper sliding surface moves, it is difficult to represent the wear analysis result with only the equivalent surface. Figure 4c shows the wear shapes of body 1 and body 2, and the sum of the wear depths of body 1 and body 2 is up to $42.0 \mu\text{m}$. Body 2 wears over a wide area because the contact position changes.

Figure 5 shows the results of the wear analysis by applying a truncation model, a fixed model, and a quasi-static model to an actual rough surface with numerous asperities. As described in Section 2.1, a part of the total contact area of the two objects is set as the analysis area, which is a square with a side length of $L = 0.889$ mm, and this analysis area is subjected to a vertical load of $1N$. The number of nodes is $n_x \times n_y = 257 \times 257$. Under the conditions in which an upper moving body with a length of $L_M = 3.6$ mm slides with a sliding distance of $S = 1.8$ mm per cycle, the wear analysis was performed for 200 cycles on two objects with a Gaussian surface, with the same material as the elastic modulus of $E_1 = E_2 = 200$ GPa, Poisson's ratio of $\nu_1 = \nu_2 = 0.3$, and wear coefficient of $k = 5 \times 10^{-5}$. Figure 5a–c show the 2D profile change in the gap between the surface pairs analyzed by the truncation model, the fixed model, and the quasi-static model. In the truncation model, the worn parts in each asperity all have the same height and the wear progresses faster than in the other two models since the wear depth is predicted to be large. The analysis model with the slowest wear progress was the quasi-static model, and although the wear depth was small, more peaks were worn than with the fixed model. In the quasi-static model, the

gap continues to change as the upper moving surface slides, and as a result, more asperities were worn than in the fixed model. Moreover, even if the asperity is in contact at any step, it does not mean that it is in contact throughout one cycle, so the pressure is distributed over several asperities. On the other hand, in the fixed model, since the point of contact does not change and it is considered to be in continuous contact at that location during the cycle, wear occurs intensively at that point.

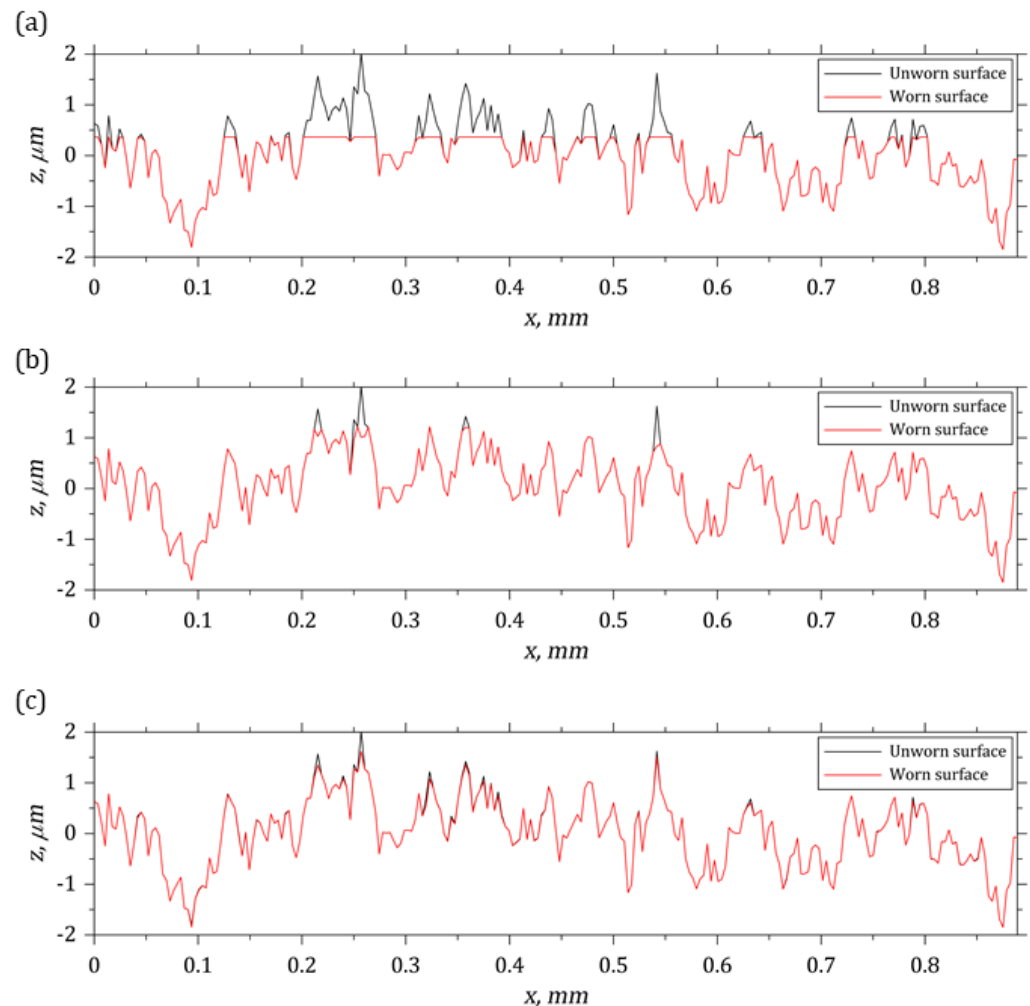


Figure 5. 2D profile of unworn and worn surface: (a) Truncation model; (b) deterministic fixed model; (c) deterministic quasi-static model.

Figure 6 shows the change in RMS roughness of the Gaussian surface from that in Figure 5 during 400 cycles. RMS roughness decreases as the peak is lowered by wear, and the decrease in RMS roughness is the largest in the truncation model. Analysis using the truncation model was performed for 210 cycles, and the reason will be explained later. In the truncation model, the fact that the point at which the slope of RMS roughness becomes smaller coincides with the point at which the number of contact asperities sharply increases indicates that an error occurs from the spherical assumption as in the single asperity wear problem described above, and the effect is increased and accumulated as the number of contact asperities increases. In addition, in the wear analysis process, the actual profile with a higher value than the spherical-fitted profile is cut, and therefore, wear occurs in more nodes than the number of nodes that should have been worn in the spherical shape. This causes the RMS roughness to decrease more rapidly. In addition, under the assumption of contact between the sphere and the rigid plane, 1.5 times the average pressure becomes the pressure at the peak point. Since the pressure gradient in the actual shape is flatter than the

pressure gradient of the rigid plane-sphere contact, the contact pressure on the worn rough surface is overestimated with the Hertz equation.

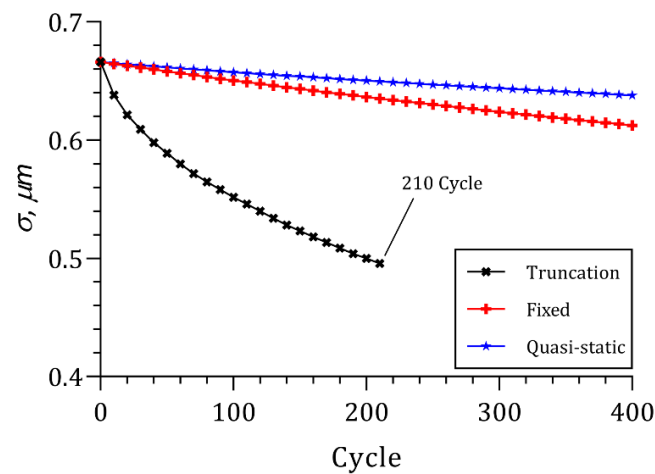


Figure 6. RMS roughness vs. wear cycle in the truncation model, deterministic fixed model, and deterministic quasi-static model.

The truncation model has the advantage of being simple and fast, but it results in unavoidable problems. Figure 7 presents a contour map showing the surface change in the wear analysis of the same Gaussian surface as that in Figure 5 from the truncation model. Since the peaks and valleys are uniformly distributed in the beginning, the intersection point of the rigid body plane and the surface profile can be well defined, and there is no big problem in finding the radius by fitting the asperity with a sphere. In each cycle, the peaks are all replaced with the same height. As the wear progresses, the number of nodes with the same height value increases and the flat area becomes wider. As this area becomes wider, the radius estimation error increases, and the accuracy of the truncation model decreases. In addition, the evenly distributed flat area gradually expands and merges with another area in the vicinity to form an irregular shape that makes it difficult to specify the center of the asperities used in the fitting process. For this reason, we considered that the accuracy of the truncation model decreased as the wear progressed, and the analysis was performed until the worn area out of the total area reached 30%. In the case of the Gaussian surface used in Figures 5–7, the analysis was stopped after 210 cycles.

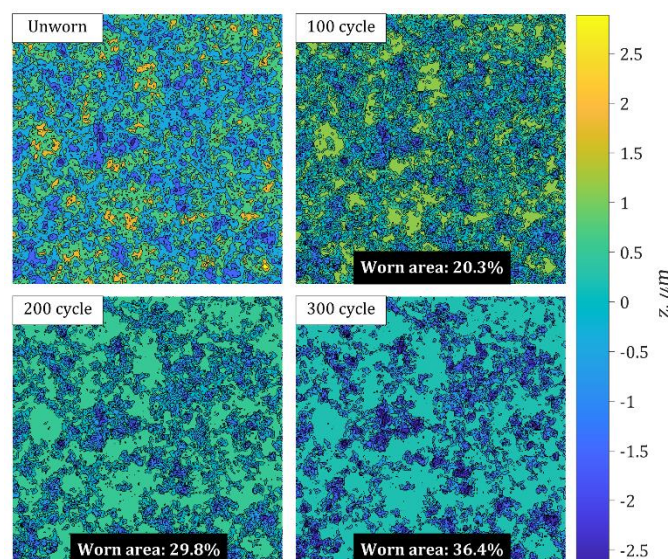


Figure 7. Surface contour as the wear cycle progresses in the truncation model.

3.2. Wear Simulation by Deterministic Quasi-Static Model

For wear analysis using the quasi-static model, an upper moving surface and a lower stationary surface were created, and the two surfaces were assumed to be symmetrical with respect to the contact surface to confirm the difference in wear depth according to the upper/lower positions. Three surfaces with different statistical parameters were analyzed to compare the wear progress according to skewness Sk and kurtosis Ku . The input values for surface generation, contact, and wear analysis conditions are shown in Tables 1 and 2.

Table 1. Rough surface generation parameters.

Parameter	Value		
	Surface 1	Surface 2	Surface 3
σ	0.67 μm	0.67 μm	0.67 μm
Sk	0	0.5	−0.5
Ku	3	4	3.3
L	0.889 mm	0.889 mm	0.889 mm
$n_x = n_y$	257	257	257
β	0.04 mm	0.04 mm	0.04 mm

Table 2. Contact and wear analysis parameters.

Parameter	Value
$E_1 = E_2$	200 GPa
$\nu_1 = \nu_2$	0.3
$H_1 = H_2$	3 GPa
F_z	3.9516 N
$k_{wear,1} = k_{wear,2}$	5×10^{-5}
S	12.78 mm
L_S	12.78 mm
L_M	3.6 mm

Figure 8a–c show the probability density functions of surfaces 1, 2, and 3, and Figure 8d–f show the generated rough surface. As shown in Figure 8a, the probability density function of surface 1 is consistent with the normal distribution, which means it can be verified that a Gaussian surface with values of $Sk = 0$, $Ku = 3$ was properly generated. The probability density function of surface 2 in Figure 8b shows a positively skewed distribution that is skewed to the left, the data are slightly concentrated at a location smaller than the mean, and the right tail of the distribution is longer. Moreover, due to the high kurtosis, the maximum value of the probability density function is higher than that of the normal distribution curve. Surface 2 in Figure 8e shows more peaks than valleys due to skewness. The probability density function of surface 3 in Figure 8c shows a negatively skewed distribution that is skewed to the right, the data are concentrated at a location higher than the mean, and the left tail of the distribution is longer. Surface 3 in Figure 8f has almost no peak and the contact surface is smooth.

3.2.1. Surface Topography Evolution

Figure 8g–i show the lower stationary surface after 250 cycles, and Figure 8j–l show the upper moving surface after 250 cycles. After 250 cycles, the peaks were removed and both surfaces became flat, showing a difference in the number and depth of the valleys. The upper moving surface is always in contact, and the sliding distance is S . In the case of the lower stationary surface, the sliding distance is L_M , as discussed in Section 2.3, because wear occurs only when the upper moving surface passes the lower stationary surface. Thus, the wear depth of the lower stationary surface is smaller, which is the cause of the difference in shape between the upper and lower surfaces. In Figure 8j–l, a wear scar is formed on the upper moving surface in the sliding direction, which is a trace left on the upper moving

surface by the asperities of the lower stationary surface. The wear scars created on surfaces 1 to 3 have different shapes depending on the characteristics of the two surfaces in contact. Since the lower stationary surface wears relatively slowly, the characteristics of the lower stationary surface affect the wear scar of the opposite surface. The wear scar is formed deepest on the upper moving surface of surface 2 because the roughness of the contact surface is the most severe due to high kurtosis and positive skewness. On the other hand, on surface 3, which has fewer asperities and is gentle, the contact area is wide and the wear depth is shallow, so the wear scar is relatively light.

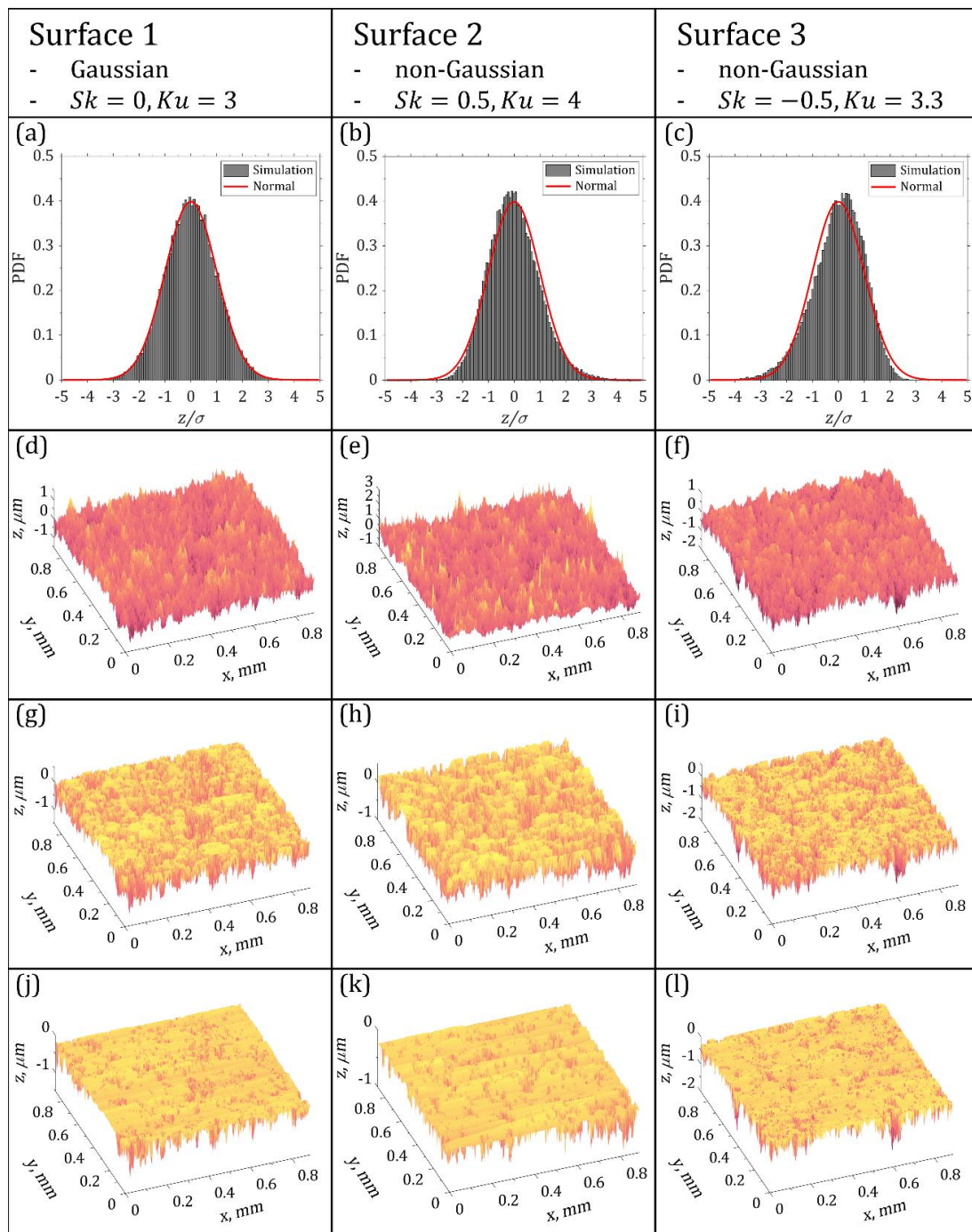


Figure 8. Gaussian and non-Gaussian surfaces for wear analysis: (a–c) Probability density functions of generated surfaces; (d–f) generated rough surfaces; (g–i) worn lower stationary surface; (j–l) worn upper moving surface.

Figure 9a shows the PDF change of the Gaussian surface. As the peaks wear out at the beginning of the cycle, the values located at the right tail of the PDF create small peaks on the PDF. As the wear progresses, the existing peak and the newly created peak are combined to become higher, and the position gradually shifts to the left. From the PDF at 20 cycles, it can be predicted that kurtosis will tend to decrease at the beginning of wear. Figure 9b shows the ACF change of the Gaussian distribution surface at 40-cycle intervals, which verifies that the rough surface is properly generated by the surface generation algorithm when compared with the theoretical ACF. The autocorrelation length β , which is the distance to the point where the ACF value becomes 0.1, is also equal to 0.04 mm. As the surface becomes flat as the wear progresses, the height values gather in a relatively similar range, and thus the ACF value indicating the degree of similarity gradually increases overall. Above 90 cycles, β is no longer definable because the ACF value does not have a value below 0.1.

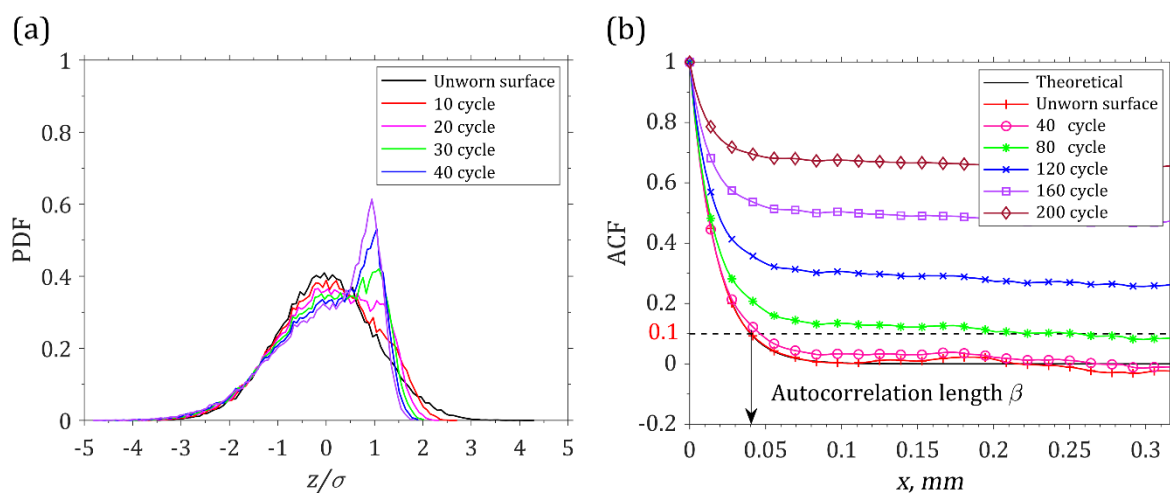


Figure 9. Evolution of functions representing rough surface properties: (a) Probability density function; (b) autocorrelation function.

3.2.2. Roughness Parameters, Contact and Wear Properties vs. Wear Cycle

We investigated the main statistical parameters of the surface and changes in contact and wear properties during 250 cycles. Figure 10a shows the change in RMS roughness of the upper and lower surfaces for three cases. As the surface wears, the RMS roughness decreases, and the wear depth of the lower stationary surface is less than that of the upper moving surface. Surface 3 has a relatively high contact area because the contact surface is blunt. Therefore, since the pressure acting on the asperities is small, the wear depth is also proportionally small according to the wear equation, and as a result, the change in RMS roughness is the smallest. Surface 2 has sharp asperities due to high kurtosis and a contact surface with few peaks because the skewness is positive. Therefore, the pressure is concentrated on the peaks of asperities, and the wear depth is deeper than that of surfaces 1 and 3, and consequently, the change in RMS roughness is the largest. Figure 10b shows the change in skewness. Since a surface with more peaks than valleys has a positive skewness, and a surface with the opposite characteristic has a negative skewness, as the peaks are removed by wear, the skewness increases in the negative direction. Surface 2 has a sharp decrease in skewness compared to other surfaces in the initial cycle because peaks are rapidly removed by high pressure due to the asperity shape. Figure 10c shows the change in kurtosis. As mentioned in Section 3.2.1, kurtosis decreases and then increases on surfaces 1 and 2 because the high asperities disappear at the initial wear cycle. After all the peaks are removed, kurtosis increases as the flat area expands. Figure 10d shows the wear depth defined as the distance between the maximum value of the unworn profile and the maximum value of the worn profile in each cycle. Severe wear and steady wear were well observed based on the point where the slope of the graph changed.

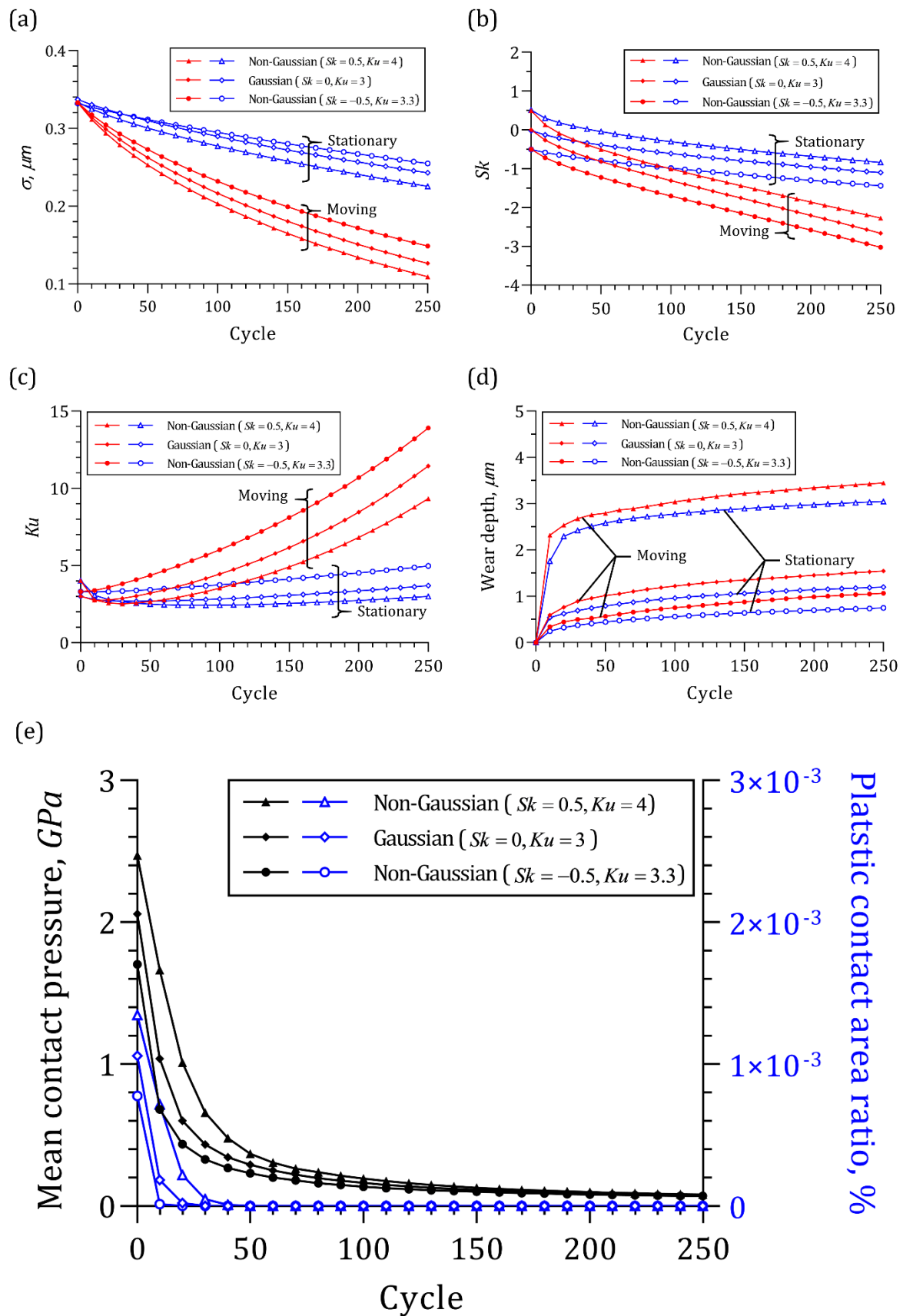


Figure 10. Parameters vs. wear cycle: (a) RMS roughness; (b) skewness; (c) kurtosis; (d) wear depth; (e) mean contact pressure and plastic contact area ratio.

Figure 10e shows the average contact pressure and plastic contact area ratio in three cases. As wear progresses, the number of contact asperities increases, so the real contact area continues to increase. Thus, the contact pressure at the contact node continues to decrease. The rapid decrease in pressure is because the peaks are concentrated under the pressure and rapidly worn. The average contact pressure is greatest on surface 2 because of the small number of peaks and the small contact area of the asperities. Since plastic contact exists only at the beginning of the cycle, where the plastic contact area to the total contact area at the beginning is 43% and plasticity occurs in most of the contact nodes, it is essential to consider plasticity in the contact analysis of rough surfaces. However, since there is no node where plasticity occurs after 40 cycles at surface 1, 70 cycles at surface 2, and 20 cycles at surface 3, there is no need to perform plastic contact analysis after a certain cycle. Although the EPP model, which is the simplest model of plasticity, is used, the efficiency will be significantly different depending on the presence or absence of plasticity analysis when a more sophisticated model is selected.

4. Conclusions

The purpose of this study is to analyze adhesion wear with a deterministic method and predict changes in surface parameters by considering the change in contact points of asperities that occur in the periodic sliding motion. The pressure distribution in the sliding process varies according to the location of the upper moving surface, and the prediction is more precise because the wear depth is evaluated at each position. To consider the characteristics of a rough surface, a very small area at the level where periodicity is established is set as the analysis area, and CGM and CC-FT are used for pressure calculation. In order to examine the effect that occurs as the contact points of asperities are changed, the data of the upper moving surface are moved over the lower stationary surface as in the actual sliding phenomenon, and the sliding wear following the Archard wear model is analyzed as a quasi-static process by dividing one cycle into small steps. In addition, the results of the truncation model and deterministic wear models are compared and analyzed.

The conclusions are as follows:

1. The simulation results of three models are analyzed and compared for the sliding wear of a plane and single asperity, and limitations of the truncation model are suggested. As a result of the analysis of sphere contact, the truncation model predicts more wear depth than the deterministic fixed model, and the truncation model shows excessive wear depth on rough surfaces. This is because, although the shape of the asperities gradually changes from the sphere during the wear process, the contact pressure is obtained as the Hertzian equation for the contact between the sphere and the plane. In addition, as the worn area increased, the error for the radius estimation accumulated, which indicates that the analysis result is not accurate.
2. Wear analysis is performed on numerically generated Gaussian, positively skewed, and negatively skewed surfaces. The sliding distance difference according to the presence or absence of movement of the surface is considered. As a result, the positively skewed surface, where the pressure concentration due to the shape of the asperities occurs the most, has the fastest decrease in RMS roughness. As the peaks on the surface disappear with wear, the skewness increases in the negative direction, and the kurtosis initially decreases and then increases.
3. In periodic sliding motion, the wear progress of the lower stationary surface is relatively slow because the sliding distance between the upper moving object and the lower stationary object is different. As a result, wear scars from asperities on the lower stationary surface appear on the upper moving surface, which is either deep or shallow depending on the surface.
4. Since the plastic contact area occupies a large proportion of the total contact area in the initial wear cycle, plastic contact must be considered in the contact analysis of rough surfaces. However, plastic contact does not occur after the contact area is sufficiently

large due to wear. Therefore, the analysis time can be shortened by performing only elastic contact analysis instead of elastic–plastic contact analysis.

This model can be applied to the analysis of wear between objects in the periodic sliding motion, such as a piston–liner, a shaft, and the bearing surface of sliding bearings. In addition, it is possible to analyze the effect of the shape of the surface more precisely with relatively better wear resistance on the rough shape of the mating surface.

Author Contributions: Conceptualization, Y.K. and Y.Y.; Methodology, Y.K., B.L., K.P. and Y.Y.; Software, Y.K. and B.L.; Validation, Y.K., B.L. and Y.Y.; Investigation, Y.K., B.L. and K.P.; Writing—original draft, Y.K.; Writing—review & editing, J.S., B.L. and Y.Y.; Visualization, Y.K., Y.C., K.P. and Y.Y.; Supervision, J.S. and Y.Y.; Funding acquisition, J.S., Y.C. and Y.Y. All authors have read and agreed to the published version of the manuscript.

Funding: This work was supported by the National Research Foundation of Korea (NRF) grant funded by the Korea government (MSIT) (No. 2022R1C1C2003523) and by the Nano-Material Technology Development Program through the National Research Foundation of Korea (NRF) funded by the Ministry of Science and ICT (No. 2020M3H4A3106186).

Institutional Review Board Statement: Not applicable.

Informed Consent Statement: Not applicable.

Data Availability Statement: Not applicable.

Acknowledgments: The authors express their sincere gratitude to all study participants.

Conflicts of Interest: The authors declare no conflict of interest.

References

- Hong, W.; Cai, W.; Wang, S.; Tomovic, M.M. Mechanical wear debris feature, detection, and diagnosis: A review. *Chin. J. Aeronaut.* **2017**, *31*, 867–882. [[CrossRef](#)]
- Holmberg, K.; Erdemir, A. Influence of tribology on global energy consumption, costs and emissions. *Friction* **2017**, *5*, 263–284. [[CrossRef](#)]
- Dumbleton, J.H.; Manley, M.T.; Edidin, A.A. A literature review of the association between wear rate and osteolysis in total hip arthroplasty. *J. Arthroplast.* **2002**, *17*, 649–661. [[CrossRef](#)]
- Garg, B.D.; Cadle, S.H.; Mulawa, P.A.; Groblicki, P.J.; Laroo, C.; Parr, G.A. Brake Wear Particulate Matter Emissions. *Environ. Sci. Technol.* **2000**, *34*, 4463–4469. [[CrossRef](#)]
- Hussein, T.; Johansson, C.; Karlsson, H.; Hansson, H.-C. Factors affecting non-tailpipe aerosol particle emissions from paved roads: On-road measurements in Stockholm, Sweden. *Atmospheric Environ.* **2008**, *42*, 688–702. [[CrossRef](#)]
- Dahl, A.; Gharibi, A.; Swietlicki, E.; Gudmundsson, A.; Bohgard, M.; Ljungman, A.; Blomqvist, G.; Gustafsson, M. Traffic-generated emissions of ultrafine particles from pavement–tire interface. *Atmospheric Environ.* **2006**, *40*, 1314–1323. [[CrossRef](#)]
- Thorpe, A.; Harrison, R.M. Sources and properties of non-exhaust particulate matter from road traffic: A review. *Sci. Total Environ.* **2008**, *400*, 270–282. [[CrossRef](#)]
- Lu, Z.; Cao, Z.; Hu, E.; Hu, K.; Hu, X. Preparation and tribological properties of WS₂ and WS₂/TiO₂ nanoparticles. *Tribol. Int.* **2018**, *130*, 308–316. [[CrossRef](#)]
- Wang, B.; Hu, E.; Tu, Z.; David, K.D.; Hu, K.; Hu, X.; Yang, W.; Guo, J.; Cai, W.; Qian, W.; et al. Characterization and tribological properties of rice husk carbon nanoparticles Co-doped with sulfur and nitrogen. *Appl. Surf. Sci.* **2018**, *462*, 944–954. [[CrossRef](#)]
- Chen, Z.; Liu, Y.; Günsel, S.; Luo, J. Mechanism of Antiwear Property Under High Pressure of Synthetic Oil-Soluble Ultrathin MoS₂ Sheets as Lubricant Additives. *Langmuir* **2018**, *34*, 1635–1644. [[CrossRef](#)]
- Ríos, J.; Quintero, D.; Castaño, J.; Echeverría, F.; Gómez, M. Comparison among the lubricated and unlubricated tribological behavior of coatings obtained by PEO on the Ti6Al4V alloy in alkaline solutions. *Tribol. Int.* **2018**, *128*, 1–8. [[CrossRef](#)]
- Vereschaka, A.; Aksenenko, A.; Sitnikov, N.; Migranov, M.; Shevchenko, S.; Sotova, C.; Batako, A.; Andreev, N. Effect of adhesion and tribological properties of modified composite nano-structured multi-layer nitride coatings on WC-Co tools life. *Tribol. Int.* **2018**, *128*, 313–327. [[CrossRef](#)]
- Antonov, M.; Afshari, H.; Baronins, J.; Adoberg, E.; Raadik, T.; Hussainova, I. The effect of temperature and sliding speed on friction and wear of Si₃N₄, Al₂O₃, and ZrO₂ balls tested against AlCrN PVD coating. *Tribol. Int.* **2018**, *118*, 500–514. [[CrossRef](#)]
- von Fieandt, L.; Fallqvist, M.; Larsson, T.; Lindahl, E.; Boman, M. Tribological properties of highly oriented Ti(C,N) deposited by chemical vapor deposition. *Tribol. Int.* **2018**, *119*, 593–599. [[CrossRef](#)]
- Kim, D.-W.; Kim, K.-W. Effects of sliding velocity and normal load on friction and wear characteristics of multi-layered diamond-like carbon (DLC) coating prepared by reactive sputtering. *Wear* **2012**, *297*, 722–730. [[CrossRef](#)]

16. Zambrano, O.A.; García, D.S.; Rodríguez, S.A.; Coronado, J.J. The Mild-Severe Wear Transition in Erosion Wear. *Tribol. Lett.* **2018**, *66*, 95. [[CrossRef](#)]
17. Laurindo CA, H.; Lepienski, C.M.; Amorim, F.L.; Torres, R.D.; Soares, P. Mechanical and Tribological Properties of Ca/P-Doped Titanium Dioxide Layer Produced by Plasma Electrolytic Oxidation: Effects of Applied Voltage and Heat Treatment. *Tribol. Trans.* **2018**, *61*, 733–741. [[CrossRef](#)]
18. Vlădescu, S.-C.; Olver, A.V.; Pegg, I.G.; Reddyhoff, T. Combined friction and wear reduction in a reciprocating contact through laser surface texturing. *Wear* **2016**, *358–359*, 51–61. [[CrossRef](#)]
19. Gu, C.; Meng, X.; Xie, Y.; Yang, Y. Effects of surface texturing on ring/liner friction under starved lubrication. *Tribol. Int.* **2016**, *94*, 591–605. [[CrossRef](#)]
20. Zhang, X.; Shen, H.; Liu, J.; Deng, S.; Li, X.; Cai, Z.; Zhu, M. An efficient numerical model for predicting the torsional fretting wear considering real rough surface. *Wear* **2015**, *344–345*, 32–45. [[CrossRef](#)]
21. Pei, X.; Pu, W.; Zhang, Y.; Huang, L. Surface topography and friction coefficient evolution during sliding wear in a mixed lubricated rolling-sliding contact. *Tribol. Int.* **2019**, *137*, 303–312. [[CrossRef](#)]
22. Prajapati, D.K.; Tiwari, M. 3D numerical wear model for determining the change in surface topography. *Surf. Topogr. Metrol. Prop.* **2018**, *6*, 045006. [[CrossRef](#)]
23. Ghosh, A.; Sadeghi, F. A novel approach to model effects of surface roughness parameters on wear. *Wear* **2015**, *338–339*, 73–94. [[CrossRef](#)]
24. Thomas, T. Computer simulation of wear. *Wear* **1972**, *22*, 83–90. [[CrossRef](#)]
25. Spedding, T.A.; King, T.G.; Watson, W.; Stout, K.J. The Pearson System of Distributions: Its Application to Non-Gaussian Surface Metrology and a Simple Wear Model. *J. Lubr. Technol.* **1980**, *102*, 495–500. [[CrossRef](#)]
26. Stout, K.; Spedding, T. The characterization of internal combustion engine bores. *Wear* **1982**, *83*, 311–326. [[CrossRef](#)]
27. Greenwood, J.A.; Tripp, J.H. The Contact of Two Nominally Flat Rough Surfaces. *Proc. Inst. Mech. Eng.* **1970**, *185*, 625–633. [[CrossRef](#)]
28. Majumdar, A.; Bhushan, B. Fractal Model of Elastic-Plastic Contact Between Rough Surfaces. *J. Tribol.* **1991**, *113*, 1–11. [[CrossRef](#)]
29. Zhu, N.; Martini, A.; Wang, W.; Hu, Y.; Lisowsky, B.; Wang, Q.J. Simulation of Sliding Wear in Mixed Lubrication. *J. Tribol.* **2007**, *129*, 544–552. [[CrossRef](#)]
30. Brink, T.; Frérot, L.; Molinari, J.-F. A parameter-free mechanistic model of the adhesive wear process of rough surfaces in sliding contact. *J. Mech. Phys. Solids* **2020**, *147*, 104238. [[CrossRef](#)]
31. Aghababaei, R.; Warner, D.H.; Molinari, R.A.J.-F. Critical length scale controls adhesive wear mechanisms. *Nat. Commun.* **2016**, *7*, 11816. [[CrossRef](#)] [[PubMed](#)]
32. Rabinowicz, E. The effect of size on the looseness of wear fragments. *Wear* **1958**, *2*, 4–8. [[CrossRef](#)]
33. Nayak, P.R. Random Process Model of Rough Surfaces. *J. Lubr. Technol.* **1971**, *93*, 398–407. [[CrossRef](#)]
34. Peklenik, J. Paper 24: New Developments in Surface Characterization and Measurements by Means of Random Process Analysis. *Proc. Inst. Mech. Eng. Conf. Proc.* **1967**, *182*, 108–126. [[CrossRef](#)]
35. He, Y.F.; Tang, J.Y.; Zhou, W.; Liao, D.R. Research on the Obtainment of Topography Parameters by Rough Surface Simulation With Fast Fourier Transform. *J. Tribol.* **2015**, *137*, 031401. [[CrossRef](#)]
36. Wang, J.; Zhu, D. *Interfacial Mechanics: Theories and Methods for Contact and Lubrication*; CRC Press: Boca Raton, FL, USA, 2019.
37. Polonsky, I.; Keer, L. A numerical method for solving rough contact problems based on the multi-level multi-summation and conjugate gradient techniques. *Wear* **1999**, *231*, 206–219. [[CrossRef](#)]
38. Clarke, A.; Weeks, I.; Snidle, R.; Evans, H. Running-in and micropitting behaviour of steel surfaces under mixed lubrication conditions. *Tribol. Int.* **2016**, *101*, 59–68. [[CrossRef](#)]
39. Lee, S.C.; Ren, N. Behavior of Elastic-Plastic Rough Surface Contacts as Affected by Surface Topography, Load, and Material Hardness. *Tribol. Trans.* **1996**, *39*, 67–74. [[CrossRef](#)]
40. Wu, J.-J. Simulation of rough surfaces with FFT. *Tribol. Int.* **2000**, *33*, 47–58. [[CrossRef](#)]
41. Wu, J.-J. Simulation of non-Gaussian surfaces with FFT. *Tribol. Int.* **2004**, *37*, 339–346. [[CrossRef](#)]
42. Liu, S.; Wang, Q.; Liu, G. A versatile method of discrete convolution and FFT (DC-FFT) for contact analyses. *Wear* **2000**, *243*, 101–111. [[CrossRef](#)]
43. Chang, W.-R.; Etsion, I.; Bogy, D.B. An Elastic-Plastic Model for the Contact of Rough Surfaces. *J. Tribol.* **1987**, *109*, 257–263. [[CrossRef](#)]